

Short range travel time geoacoustic inversion with vertical line array

Yong-Min Jiang and N. Ross Chapman

*School of Earth and Ocean Sciences, University of Victoria, PO Box 3055 Victoria,
British Columbia, Canada, V8W 3P6
minj@uvic.ca, chapman@uvic.ca*

Peter Gerstoft

*Marine Physical Laboratory, Scripps Institution of Oceanography, La Jolla, California 92093-0238
gerstoft@ucsd.edu*

Abstract: This paper presents travel time geoacoustic inversion of broadband data collected on a vertical line array at short range of 230 m during the Shallow Water 2006 experiments. A ray-tracing method combined with a hybrid optimization algorithm that utilizes differential evolution and downhill simplex was used for the inversion of sediment properties. The ocean sound speed profile and geometric parameters were inverted prior to the sea bottom properties to account for the temporally variable ocean environment. The sediment sound speed and thickness estimates are consistent with *in situ* measurements and matched-field inversion results of longer-range data from the experiment.

© 2008 Acoustical Society of America

PACS numbers: 43.30.Pc, 43.60.Pt [WC]

Date Received: March 17, 2008 **Date Accepted:** June 9, 2008

1. Introduction

Many geoacoustic inversion techniques have been developed and successfully implemented to estimate sea bottom properties. Most of the research assumed that the ocean sound speed profile (SSP) was spatio-temporally invariant. However, the ocean SSP has significant impact on matched-field geoacoustic inversion (MFI),¹ and MFI performance is improved by including ocean sound speed variability in the inversion.^{2,3}

The objective of this work is to report travel time geoacoustic inversion in a time varying ocean environment. The data were collected on the Marine Physical Laboratory vertical line array (MPL-VLA1) during the Shallow Water 2006 (SW06) experiments. SW06 was a multi-disciplinary, multi-institution experiment that was carried out near the shelf break on the New Jersey continental shelf from mid-July to mid-September, 2006.⁴ The objectives of the geoacoustic inversion component of SW06 were to estimate seabed properties at a common interest site through different approaches (i.e., using different acoustic field information and inversion algorithms), compare the limitations of each method, and understand the influence of the oceanographic variability on the estimated parameters and their uncertainties.

The oceanographic variation was observed from the SSPs measured at the source position. In order to reduce sea bottom estimation uncertainties arising from temporal variation of the ocean environment, the ocean SSP was parameterized in terms of empirical orthogonal functions (EOFs) and their coefficients were inverted prior to the geoacoustic inversion. The acoustic model used here is based on ray theory. The inversion combined the global optimization algorithm differential evolution⁵ and the local optimization algorithm downhill simplex⁶ (adaptive simplex differential evolution, ASDE) to estimate parameters of a simple geoacoustic model. The experimental design with multiple source depths and multiple hydrophones at close range provided the multiplicity of sub-bottom acoustic paths to resolve the sediment properties.

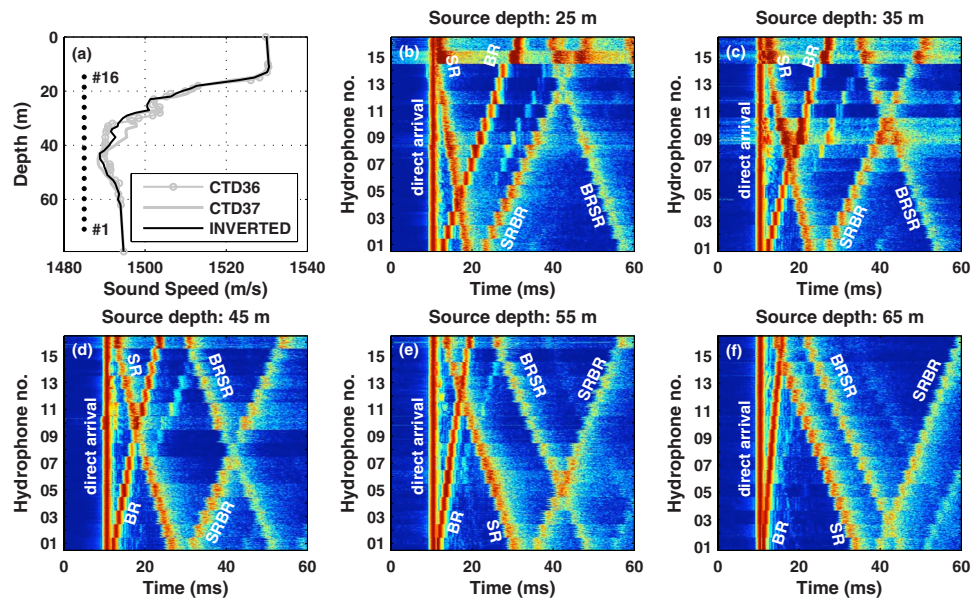


Fig. 1. (Color online) (a) CTD36, CTD37 and inverted SSP for the 25 m source data. The black dots indicate the hydrophone positions in the water. (b)-(f) Normalized matched filtered LFM signals collected on 16 hydrophones for the 25–65 m source depths.

2. Short range acoustic experiment

The data were collected on 31 August on MPL-VLA1 that was deployed at ($39^{\circ}1.4771'N$, $73^{\circ}2.259'W$). Sixteen hydrophones were equally spaced on the array with a separation of 3.75 m, and the bottommost hydrophone (No.1) was 8.2 m above the sea floor. The source was deployed from the R/V Knorr, lowered down in the water column from 15 to 65 m in 10 m intervals, and was held for 5 min at each depth. During the signal transmission, the ship was maintained at ~ 230 m from the VLA using dynamic positioning. The transmitted signal was a 1 s 1500–4500 Hz mid-frequency linear frequency modulation pulse, repeated each second.

The bathymetry between the source and MPL-VLA1 is almost flat with 79.6 m at the source and 79.0 m at MPL-VLA1. CTDs (conductivity-temperature density) were measured immediately before (CTD36) and after (CTD37) the experiment. The time between the two CTDs was 45 min. The derived SSPs shown in Fig. 1(a) have almost iso-velocity layers at the top and lower portions of the water column, and a strong negative downward refraction thermocline from 15–30 m. The middle part of the SSP shows strong time variation.

Mid-frequency LFM signals received at all of the hydrophones on the VLA were matched filtered by the replica source pulse. To eliminate undesired noise in the data, the signal bandwidth was limited to 1500–3800 Hz. The envelopes of the normalized matched filtered signals (dB) are shown in Figs. 1(b) to 1(f). Each panel represents 1 min signals (60 transmissions stacked vertically) received at all hydrophones at the source depths from 25 to 65 m. The 60 transmissions shown for each hydrophone give a qualitative impression of the signal variability.

Ray tracing⁷ was used to identify the direct, bottom reflected (BR), surface reflected (SR), surface reflected-bottom reflected (SRBR), and bottom reflected-surface reflected (BRSR) arrivals. For all the source depths, the BR paths at the hydrophones in the bottom portion of water column have small travel time variations. SR paths at the hydrophones in the top portion of the water column have greater amplitude and travel time variations due to source

motion, sea surface roughness, and relatively larger hydrophone position variation. Sub-bottom reflections are observed between BR and SR/SRBR paths for the 45, 55, and 65 m sources, or between BR and SRBR for the 25 and 35 m sources.

Multiple direct arrivals were observed for the sources and receivers in the thermocline (15–30 m) due to the strong negative gradient and the existence of microstructures in the thermocline layer. The direct path amplitude from the ray tracing was not accurate due to the multi-path interference, so there was no attempt to extract bottom reflection coefficients. Instead we used the travel times for inversion.

3. Acoustic model, objective function, and bottom parameterization

A range independent ray-tracing model to invert for the sub-bottom geoacoustic profile was developed for this study. The model searched for the ray parameter $[\cos(\varphi(z))/c(z)]$, where φ , c , and z are grazing angle, sound speed and depth for an eigenray that connected the source and receiver within any given range tolerance (here 0.005 m). The inversion was done in two stages, the first to invert for the SSP and geometry (water depth, range, source and receiver depths, array tilt) of the experiment, and then the geoacoustic parameters.

The inversion algorithm is a hybrid optimization method, adaptive simplex differential evolution ASDE. The local optimization downhill simplex algorithm⁶ is embedded in the global optimization algorithm differential evolution.⁵ The perturbation size in the downhill simplex is adaptively adjusted according to the models being accepted. Control parameters for ASDE are: population size⁵ is 20 times of the number of parameters to be inverted; mutation factor is 0.8; crossover factor is 0.8; and the perturbation number in the downhill process is 5.

The objective function compares the differences of the modeled ray travel time $T_{i,j}(\bar{m})$ and the measured ray travel time $t_{i,j}$: $E(\bar{m}) = \sum_{i=1}^{N_L} \sum_{j=1}^{N_H} (t_{i,j} - T_{i,j}(\bar{m}))^2$, where \bar{m} is the vector of model parameters to be inverted; N_H is the number of hydrophones; and N_L is the number of reflectors used in the inversion. When tracing rays reflected from ocean surface and bottom, $N_L=2$ while $t_{i,j}$ represents the time differences between BR paths and direct arrivals, and the time differences between SR paths and direct arrivals. When tracing rays reflected from the sub-bottom layers, N_L equals the number of layers and $t_{i,j}$ represents the time difference between the sub-bottom reflection path and the corresponding BR path.

The ability to resolve bottom structures is limited by the time resolution of the transmitted signal and the strength of the sub-bottom reflections. The bottom parameterization was based on resolvable sub-bottom reflections. Figure 1 shows a strong bottom reflection for all five source depths (no sub-bottom reflection was identified for the 15 m source). For the 55 and 65 m source depths, multiple sub-bottom layer reflections are also revealed by a weak signal enhancement technique (similar to automatic gain control) that was applied to the matched filtered time series. Figure 2(b) shows the enhanced 55 m source depth signals. The multiple hydrophone geometry provided a multiplicity of acoustic paths in the sub-bottom layer for the travel time inversion.

4. Effect of water column SSP variations to the received signal

Figure 2(a) shows the envelope of the matched filtered time series for the 25 m source depth. The resolution of the signal is about 0.5 ms. Figure 2(a) compares the travel time predictions using the previously known values for the experimental geometry and the two ocean SSP measurements, and the inverted experimental geometry and SSP. The travel time difference between predictions using CTD36 or CTD37 for hydrophones 8–14 are up to 2 ms. This is more than the resolution of the signal, thus the measured SSPs are not accurate enough for the geoacoustic inversion.

The direct, sea surface, and bottom reflection paths in the water column were used to invert for the experimental geometry and ocean SSP. Two steps were taken to improve the estimates of these parameters for the geoacoustic inversion. First, the 65 m source signals were used to invert for the experimental geometry using CTD37, because this CTD was obtained immediately after the 65 m source transmission. The inverted values were 79.2 m for water

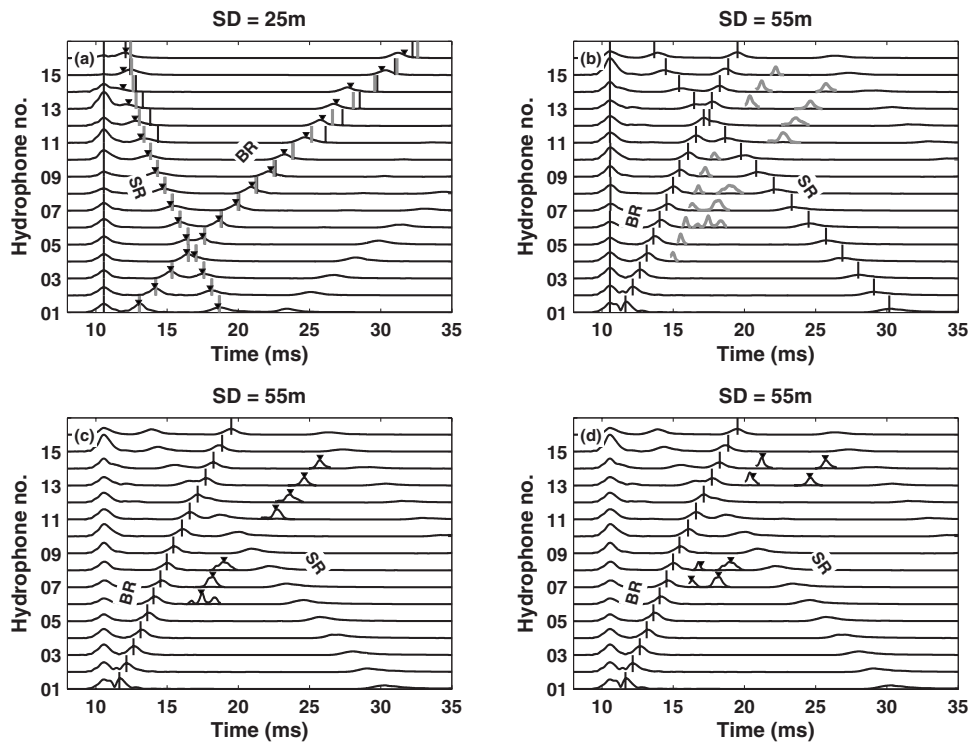


Fig. 2. Received waveforms for the (a) 25 m and (b)–(d) 55 m source with enhanced sub-bottom reflections for the 55 m source data [gray curves in (b)]. The travel times superimposed in (a) are obtained using CTD36 (vertical gray lines), CTD37 (vertical black lines), and inverted SSP (black triangles); and in (b) using the inverted ocean SSP (vertical lines). The travel times produced by inverted geoacoustic parameters for (c) one-layer model and (d) two-layer model are marked in black triangles.

depth, 233.4 m for range, 64.6 m for source depth. The search bounds were [78,81] m, [220,240] m, and [60,70] m, respectively. Second, SSPs for the other source depths were parameterized by EOFs,³ and the EOF coefficients were inverted using the established geometric parameters. The inverted SSP for 25 m source data is shown in Fig. 1(a), and the travel time predictions obtained using the inverted geometry and SSP for the 55 m source data are also shown in Fig. 2(b).

5. Inversion of sediment sound speed and layer thickness

The sub-bottom reflection in the 25–65 m source data which is apparent in Fig. 1 suggests the existence of a strong reflector in the bottom. The inversion first assumes a single sediment layer over a half space. The inversion results and the corresponding two way travel times (TWTs) are shown in Table 1. For the 55 and 65 m source data, a two-layer sediment over a half space was

Table 1. Travel time inversion results for one-layer over half space model.

Parameter	Source depth				
	25 m	35 m	45 m	55 m	65 m
Layer thickness (m)	21.5	20.6	22.3	22.3	20.4
Sound speed (m/s)	1609	1597	1600	16001	1584
TWT (ms)	26.7	25.8	27.9	27.9	25.8

Table 2. Travel time inversion results for two-layer over half space model.

Source depth	Layer I		Layer II	
	Sound speed	Layer thickness	Sound speed	Layer thickness
55 m	1581 m/s	11.9 m	1602 m/s	9.1 m
65 m	1584 m/s	14.5 m	1611 m/s	8.4 m

also used in the inversion. The results are shown in Table 2. In all the inversions, the search bounds were 1550–1700 m/s for sound speed and 5–30 m for the layer thickness

Sediment sound speed and layer thickness estimates of a one-layer model for all five source depths are consistent with each other (see Table 1). For the two-layer model, Table 2, the sound speed estimates are consistent with each other, and the average sound speed is consistent with the one-layer inversion results. The estimated values provide accurate predictions of the travel times of the sub-bottom reflections [Figs. 2(c) and 2(d)]. The estimates are also consistent with the results of matched-field inversion of longer range data along the same radial path from MPL-VLA1.^{2,3} The inverted sound speeds represent the average sound speeds in the layers.

The SW06 experiment site has been extensively surveyed previously so that a large amount of geological and geophysical ground truth information and oceanographic observations are available. Many geoacoustic inversion studies have been done on the New Jersey Shelf previously. Due to the variability of the seabed properties from location to location,⁸ we only compare our estimates with most recent relevant works^{8–10} near MPL-VLA1. Overall, the sound speed estimates are consistent with *in situ* sound speed measurements⁹ made about 250 m from MPL-VLA1 (1615±9 m/s and 1598±11 m/s) in the frequency band 2–11 kHz. The combination of sediment sound speed and layer thickness is also consistent with chirp seismic reflection data in terms of two way travel time (26.1±0.5 ms) from the sea bottom down to the “R” reflector.⁸

6. Conclusion

Travel time geoacoustic inversion was applied to VLA data collected at a source range of 230 m for a site on the New Jersey continental shelf. The short-range, varying-source-depth and VLA geometry provided wide grazing angle coverage of bottom interaction, as well as a multiplicity of sub-bottom propagation paths through the layers for the geoacoustic inversion. The effect of time varying ocean sound speed was mitigated by inverting for the ocean SSPs prior to the geoacoustic inversion. The hybrid optimization algorithm ASDE is efficient for estimating the model parameters.

Acknowledgments

This work is supported by the Office of Naval Research under Grant Nos. N00014-05-1-0264 and N00014-03-1-0131. The authors would like to thank Dr. William S. Hodgkiss, for the acoustic data, Dr. David Knobles for the navigation data, and Dr. John Goff for the chirp seismic reflection data.

References and links

- ¹M. Siderius, P. L. Nielsen, J. Sellschopp, M. Snellen, and D. Simons, “Experimental study of geo-acoustic inversion uncertainty due to ocean sound-speed fluctuations,” *J. Acoust. Soc. Am.* **110**, 769–781 (2001).
- ²C.-F. Huang, P. Gerstoft, and W. S. Hodgkiss, “Effect of ocean sound speed uncertainty on matched-field geoacoustic inversion,” *J. Acoust. Soc. Am.* **124**, EL162–EL168 (2008).
- ³Y.-M. Jiang and N. R. Chapman, “Bayesian geoacoustic inversion in a dynamic shallow water environment,” *J. Acoust. Soc. Am.* **123**, EL155–EL161 (2008).
- ⁴D. J. Tang, J. Moum, J. Lynch, P. Abbot, R. Chapman, P. Dahl, T. Duda, G. Gawarkiewicz, S. Glenn, J. Goff, H. Graber, J. Kemp, A. Maffei, J. Nash, and A. Newhall, “Shallow Water ’06-A joint acoustic propagation/nonlinear internal wave physics experiment,” *Oceanogr.* **20**, 156–167 (2007).
- ⁵R. Storn and K. Price, “Differential evolution—a simple and efficient adaptive scheme for global optimization over continuous spaces,” Technical Report No. TR-95-012, ICSI, March 1995.
- ⁶W. H. Press, S. A. Teukolsky, W. T. Vetterling, and B. P. Flannery, *Numerical Recipes in Fortran*, 2nd ed.

(Cambridge University Press, Cambridge, 1992), pp. 402–406.

⁷M. B. Porter and Y.-C. Liu, “Finite element ray tracing,” in *Theoretical and Computational Acoustics*, edited by D. Lee and M. H. Schultz (World Scientific, Singapore, 1994), Vol. 2, pp. 947–953.

⁸J. A. Goff, B. J. Kraft, L. A. Mayer, S. G. Schock, C. K. Sommerfield, H. C. Olson, S. P. S. Gulick, and S. Nordfjord, “Seabed characterization on the New Jersey middle and outer shelf: Correlability and spatial variability of seafloor sediment properties,” *Mar. Geol.* **209**, 147–172 (2004).

⁹J. Yang, D. J. Tang, and K. L. Williams, “Direct measurement of sediment sound speed using SAMS in SW06,” *J. Acoust. Soc. Am.* **124**, EL116–EL121 (2008).

¹⁰B. J. Kraft, I. Overeem, C. W. Holland, L. F. Pratson, J. P. M. Syvitski, and L. A. Mayer, “Stratigraphic model predictions of geoacoustic properties,” *IEEE J. Ocean. Eng.* **31**, pp. 266–283 (2006).